Demonstrating an *In Situ* Topological Band Transition in Cylindrical Granular Chains

R. Chaunsali,[1] E. Kim,[1,2] A. Thakkar,[3] P. G. Kevrekidis,[4] and J. Yang[1,*]
[1]*Aeronautics and Astronautics, University of Washington, Seattle, Washington 98195-2400, USA*
[2]*Division of Mechanical System Engineering & Automotive Hi-Technology Research Center, Chonbuk National University, 567 Baekje-daero, Deokjin-gu, Jeonju, Jeonbuk, 54896, Republic of Korea*
[3]*Mechanical Engineering, University of Washington, Seattle, Washington 98195-2400, USA*
[4]*Department of Mathematics and Statistics, University of Massachusetts, Amherst, Massachusetts 01003-4515, USA*
(Received 17 February 2017; published 14 July 2017)

We numerically investigate and experimentally demonstrate an *in situ* topological band transition in a highly tunable mechanical system made of cylindrical granular particles. This system allows us to tune its interparticle stiffness in a controllable way, simply by changing the contact angles between the cylinders. The spatial variation of particles' stiffness results in an *in situ* transition of the system's topology. This manifests as the emergence of a boundary mode in the finite system, which we observe experimentally via laser Doppler vibrometry. When two topologically different systems are placed adjacently, we analytically predict and computationally and experimentally demonstrate the existence of a finite-frequency topologically protected mode at their interface.

DOI: 10.1103/PhysRevLett.119.024301

Introduction.—Topological insulators (TIs) constitute an intense area of recent interest within condensed matter physics. TIs support directional electron transport on their surface, and this transport is immune to defects [1]. The existence of such a surface state has a remarkable correspondence to the nontrivial topological invariants of the bulk of TIs [2]. Therefore, by knowing the topology of the bulk, one can predict the response on the surface or edge of the material. This response is robust against defects on the surface as long as the topology of the bulk is preserved. Such topological characterization has naturally emerged as a tool to design novel mechanical structures with unconventional vibration properties on their surfaces [3–8]. The study of these mechanical structures not only realizes the topological phenomenon in easily controllable and observable macroscale systems but also has potential to shape a new design paradigm for structural applications, such as vibration isolation and energy harvesting [9]. At the same time, the paradigm of TIs has had a significant impact in other areas, e.g., linear and nonlinear optics [10–14].

A dimer system such as the 1D Su-Schrieffer-Heeger (SSH) model provides the basic framework to understand band topology [15–18]. The direct mechanical analogue of such a dimer has been recently suggested [19]. This system has a phononic band gap near zero frequency and, in turn, can support *zero-frequency* topological modes. Deviating from this model, one can also arrive at a mechanical dimer that results in a non-zero-frequency band gap, potentially leading to *finite-frequency* topological modes [20]. This could be achieved by tailoring the on-site potentials in the standard SSH model. Such a system would be especially interesting, as it would enable us to understand how the topological framework can be used to predict and tailor energy localization on the edges or interfaces of a structure. To study this phenomenon in detail, one would ideally need a system that allows a *smooth* control over its topological characteristics, in order to closely observe its effects on the vibration response of the structure. Achieving such tunability is extremely challenging in experimental settings, since it requires well-controlled, *in situ* manipulation of either the mass or stiffness. Changing the masses of the dimer lattice demands manual reassembly of the systems' constituents [21,22]. Altering the stiffness values via external couplings, e.g., magnetoelastic [23], electroelastic [24], and photoelastic [25] interactions, could make the system cumbersome for structural uses. The need of precise actuation and measurement adds up to this challenge. This explains why an *in situ* topological band transition for finite-frequency elastic vibrations has not been demonstrated experimentally. A design that can address this challenge would not only contribute to our general understanding of topological mechanical systems; it also holds promise towards catalyzing the implementation of stand-alone structures with tunable energy localization characteristics.

For this purpose, we use a granular system made of cylindrical particles interacting through the Hertz contact law [26]. This system is highly tunable in that the interparticle stiffness can be changed simply by altering the contact angles between cylinders [27]. Such a versatile structure has been recently exploited for manipulating stress waves in linear [28], linear time-dependent [29], and nonlinear media [30]. To overcome the experimental challenges with regard to controlling the contact angles and conducting precise measurements, we devise an experimental setup of a tunable, stand-alone cylindrical particle system. This involves 3D-printed enclosures intended to support and tune the granular chain and to facilitate particles' velocity measurements through a laser Doppler

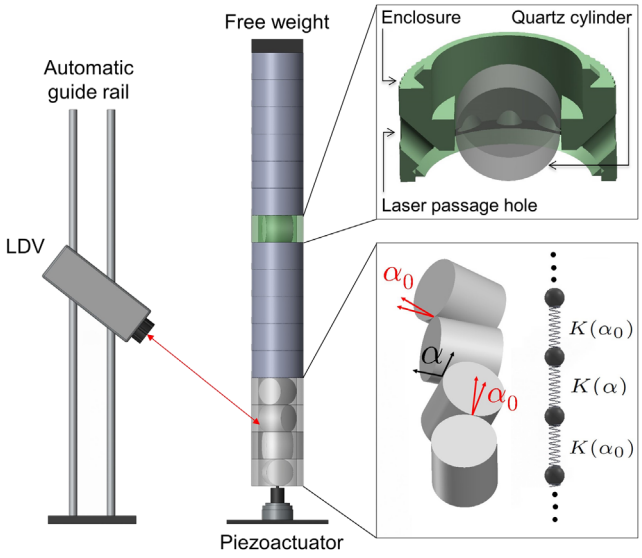

FIG. 1. Schematic of the experimental setup. The top inset illustrates a cut section of the 3D-printed enclosure. The bottom inset shows the contact angles in the dimer chain and the representative spring-mass system.

vibrometer (LDV). Using this tabletop setup, we validate the *in situ* topological band transition in the system by detecting the emergence of an experimentally measured boundary mode. We further demonstrate the existence of a topologically protected mode at the interface of two topologically distinct granular chains. Last, we theoretically calculate the frequency of the topologically protected mode using symmetries in its shape and show that it has an excellent agreement with numerics and experiments.

Experiment and numerical setup.—The experimental setup consists of a chain of short cylinders placed inside 3D-printed enclosures stacked vertically (Fig. 1). Each enclosure along with its cylinder can be independently rotated about its central axis to change the stacking angles of the particles. We maintain periodically varying two contact angles α_0 and α, such that the system resembles a dimer configuration. To demonstrate the topological transition, we fix α_0 to 20° and vary only α from 5° to 40°. The chain is composed of 27 cylinders, and all cylinders are made of fused quartz (Young's modulus $Y = 72$ GPa, Poisson's ratio $\mu = 0.17$, and density $\rho = 2187$ kg/m^3) with identical diameter and a length of 18 mm. A piezoactuator excites the bottom of the chain to send a frequency sweep signal from 3 to 30 kHz. A free weight (25 N) is placed on the top of the chain to provide initial static compression to restrict the system dynamics to the linear regime. We track the velocity of each cylinder using an LDV mounted on a guide rail. Note that we have judicially designed the enclosure to facilitate the passage of the laser beam emanating from the LDV in various angles (top inset in Fig. 1).

We use a discrete element method to model the system dynamics [31]. We represent the cylinders by lumped masses and the contacts by springs following the Hertz contact law. The force between the ith and $(i+1)$th cylinders can be written as $F_i = \beta(\alpha_i)[\delta_i + u_i - u_{i+1}]^{3/2}$, where $\beta(\alpha_i)$ is the stiffness coefficient for the contact angle of α_i; δ_i is the initial static compression due to the free weight; u_i and u_{i+1} denote the dynamic displacements of the ith and $(i+1)$th cylinders in the longitudinal direction, respectively (see Supplemental Material for details [32]). If $|u_i - u_{i+1}| \ll \delta_i$, as is the case here, we can linearize the contact law. Hence, the contact between the ith and $(i+1)$ th cylinders can be assigned to a linear stiffness coefficient, $K(\alpha_i) = \frac{3}{2}\beta(\alpha_i)\delta_i^{1/2}$. This means that a dimer configuration with alternating α_0 and α angles can be represented by a lumped mass model with linear stiffness coefficients $K(\alpha_0)$ and $K(\alpha)$, varying along the chain (bottom inset in Fig. 1).

For an infinitely long dimer chain, it is straightforward to establish a linear dispersion relation and calculate the edges of Bloch bands [34]. For a finite lattice, however, we expect to observe boundary effects. To this end, we perform the relevant eigenvalue analysis. For an N particle chain, we use $u = [u_1, u_2, u_3, \ldots, u_N] = U\exp(j\omega t)$, where U and ω represent amplitude of displacement vector and angular frequency, respectively, t is the time, and j is an imaginary unit. Thus, by neglecting dissipation in the system, we obtain $\Lambda U = \omega^2 m U$, where m is the particle mass and Λ is a $N \times N$ tridiagonal matrix consisting of stiffness coefficients $K(\alpha_0)$ and $K(\alpha)$. This finite system also accounts for the boundary condition of the finite system. Specifically, we fix the boundaries by choosing stiffness values $K_a = 2.78 \times 10^7$ N/m and $K_w = 1.62 \times 10^7$ N/m at the beginning (actuator side) and the end of the chain, respectively, to match the experimental data [32]. Using this finite setup, we evaluate eigenfrequencies and eigenmodes of the system in comparison with analytical and experimental data.

Results and discussions: Topological band transition in infinite lattices.—We first investigate the topological characteristics of the infinite dimer lattices. Figure 2 shows three dimer configurations that represent a topological band transition within our system. Theoretically obtained Bloch dispersion curves are plotted below, showing acoustic (lower) and optical (upper) branches [32]. A frequency band gap spans from $(1/2\pi)\sqrt{2K(\alpha_0)/m}$ to $(1/2\pi)\sqrt{2K(\alpha)/m}$, and the upper band edge of the optical band is at $(1/2\pi)\sqrt{2[K(\alpha_0) + K(\alpha)]/m}$. We notice that if α increases, the frequency band gap first closes at $\alpha = \alpha_0$ and then opens again. In this process, Bloch eigenmodes on the edges of the band gap are also flipped [see the change between $[1, 1]$ and $[1, -1]$ in Figs. 2(a) and 2(c)]. This indicates a typical topological band transition in our system as a function of the angle α. The system shifts between distinct dimer configurations that cannot be transformed to each other without closing the band gap. The mathematical quantification of this notion can be made by calculating the so-called Zak phase for each band; see Supplemental Material [32] for detailed calculations.

One notices that the Zak phase of a band directly relates to the symmetry types of Bloch eigenmodes at its lower

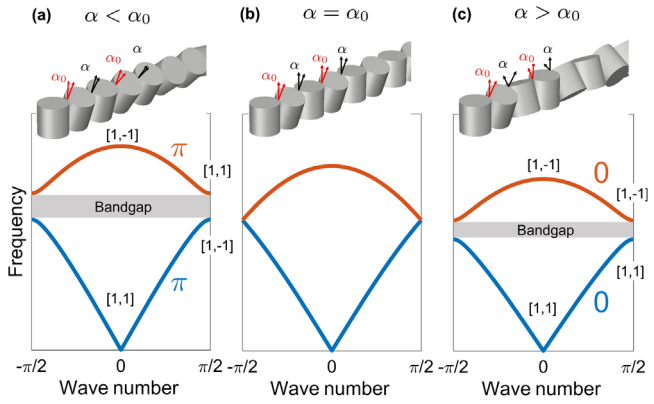

FIG. 2. Representative configurations of the infinite dimer chain to show its topological band transition as a function of α. (a), (b), and (c) include the Bloch dispersion curves for $\alpha < \alpha_0$, $\alpha = \alpha_0$, and $\alpha > \alpha_0$, respectively. Bands are marked with the corresponding topological indices (0 and π) and the Bloch eigenmodes on their edges ([1, 1] and $[1, -1]$ for symmetric and antisymmetric oscillations in the dimer unit cell, respectively).

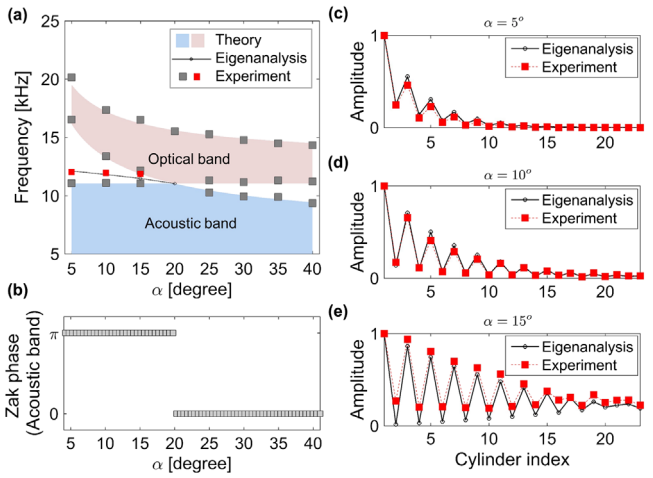

FIG. 3. Topological transition and emergence of a boundary mode in the finite system. (a) Frequency spectrum evolution as a function of α. Extracted experimental data (gray markers) match the edges of theoretical bulk bands (shaded area). Also, experiments (red markers) show the emergence of a boundary mode inside the band gap, which follows the trend of numerical simulations (black curve). (b) Zak phase of the band gap and its transition at $\alpha = \alpha_0$. (c)–(e) Numerical (black markers) and experimental (red markers) boundary mode profiles in terms of normalized velocity amplitude at $\alpha = 5°$, 10°, and 15°.

and upper band edges. The Zak phase of 0 indicates the same symmetry type [see Fig. 2(c), where the Bloch eigenmodes remain the same within the branch]. On the other hand, the Zak phase of π implies the formation of the opposite symmetry type within a band [Fig. 2(a), where the Bloch eigenmodes are flipped]. We evidently see the topological characteristics of a band gap are linked to the sum of the Zak phases of all the bands below the gap [35]. Therefore, the change in the Zak phase of the acoustic band confirms the *in situ* topological transition of our infinite lattice system.

Emergence of boundary mode in finite lattices.—The topological nature of bulk band gaps observed for an *infinite* lattice manifests itself through the emergence of boundary mode(s) inside the band gaps for a *finite* lattice (i.e., the principle of bulk-boundary correspondence) [1]. Therefore, we expect the existence of a boundary (local or edge) mode in the current topologically nontrivial dimer configurations. We extract the cutoff frequencies and the local mode information from experimental data with α varying from 5° to 40° in steps of 5° (see Supplemental Material [32] for details). Figure 3(a) summarizes the modal frequencies of the system as we vary α. Shaded areas denote modes corresponding to acoustic and optical branches of dispersion curves, constructed theoretically. We observe an excellent match of the experimental data (gray square markers) with the edges of the theoretical bands. This successfully demonstrates the band gap closing and opening mechanism in our tunable system.

Because of the finite size of the chain, we experimentally observe a local mode residing inside the band gap (red square markers for $\alpha < \alpha_0$). Black curve data, obtained through the numerical eigenvalue analysis, follow the same trend. These are boundary modes localized in the front of the chain, which are not witnessed when $\alpha > \alpha_0$. The emergence of these modes from all configurations that satisfy $\alpha < \alpha_0$ complies with the change in the band topology at $\alpha = \alpha_0$. In Fig. 3(b), we plot the Zak phase of the acoustic band as a function of α to support the aforementioned argument.

In Figs. 3(c)–3(e), we show the normalized velocity profiles of the boundary modes extracted from the experiments and the eigenanalysis. These exponentially decaying profiles match closely between experiments and numerics. The localization length, however, increases as we move from $\alpha = 5°$ to $\alpha = 15°$. This can be explained by extending the intuitive arguments in Ref. [36], according to which the localization length depends on the stiffness ratio as $\xi \propto 1/\ln[K(\alpha)/K(\alpha_0)]$. Therefore, the localization length becomes large as we increase α for $\alpha < \alpha_0$, and it is natural to expect that the mode becomes extended and is *lost* inside the band in the limit of $\alpha \to \alpha_0$.

We note that the study of these boundary modes, i.e., the *gap modes* in classical lattices, can be traced back to the pioneering work of Wallis [37]. He extensively explored the effect of finite boundaries and defects on the spectrum of ordered lattices in terms of the generation of gap modes. However, the novelty of the first part of this work is that we have kept the boundary conditions and the length of the system the same and experimentally demonstrated how the change in bulk properties reflects in the emergence of a finite-frequency boundary mode as per the topological band theory for 1D dimers.

Topological defect and protected modes.—We now study the ramifications of having two topologically different dimer configurations connected to each other. We assemble two dimer chains both with $\alpha_0 = 10°$ (hard) and $\alpha = 20°$ (soft), which connect with each other in mirror symmetry, such that

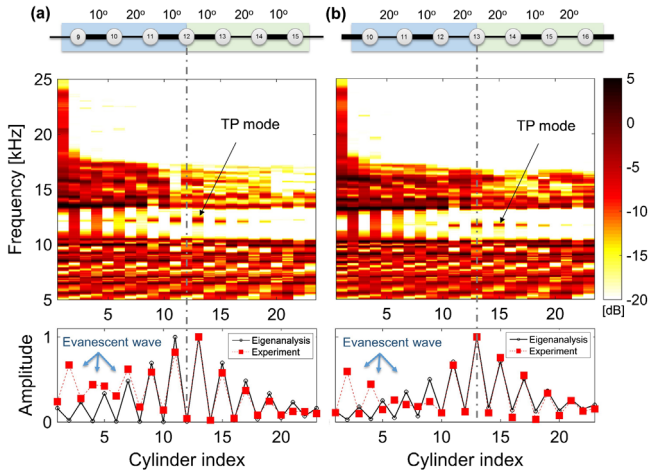

FIG. 4. Topologically protected modes arising from dimer configurations with (a) *hard-hard* and (b) *soft-soft* interfaces. Below are PSD plots obtained from the particles' velocities measured experimentally. At the bottom are the TP mode shapes extracted from experiments (red markers) and eigenanalysis (black markers).

we introduce a topological defect at their interface (see the top panels in Fig. 4 and also Refs. [8,38] for similar settings). The connecting interface can be of two types: 10°–10° or 20°–20°, representing *hard-hard* and *soft-soft* interfaces, respectively. To understand why this defect is topological and how it is different from a trivial defect, we present the following argument. Suppose we can modify any interparticle contact stiffness along the chain. Now, in a dimer system, a topologically *trivial* defect can be introduced by going to the desired location in space and changing the stiffness locally. Similarly, the argument can be made that if there is a trivial defect, we can go to the defect site and perturb the stiffness locally to restore the original defect-free dimer configuration. However, the case of a topologically *nontrivial* defect is special in that it cannot be straightforwardly reverted to such a defect-free scenario through a *compact* (i.e., *local*) perturbation. In other words, if one tries to remove the topological defect by changing the local stiffness, one can see that it is not possible unless *all* stiffness values on one side of the chain are modified (i.e., a *noncompact* perturbation). In essence, a topological defect can be removed only by changing the topology of one side of the configurations adjacently placed. Therefore, the vibration mode caused by this defect is topologically protected and robust against local perturbations around the interface location (see Supplemental Material for details [32]).

To demonstrate the topologically nontrivial modes, we follow the same procedure as mentioned in the earlier section for the experimental study. A piezoactuator is used for sending a frequency sweep signal from one end. It is understood that if a vibration mode caused due to a defect is localized in the middle of the chain, it is not easy to excite it using the input signal sent from the end of the chain. However, our current system is short enough that the topologically protected (TP) mode—localized in the middle of our short chain—can still be excited by coupling it to the evanescent waves inside the band gap. In this way, we detect the existence of TP modes for hard-hard and soft-soft configurations (Fig. 4). Power spectral density (PSD) plots are obtained experimentally by performing Fourier transformation on the temporal velocity profiles of all particles in each chain. As indicated by the arrows, we can evidently observe the existence of the TP modes in both cases. In the bottom panel, we show the extracted normalized mode shapes from the experimental data, which agree with the corresponding computed eigenmodes. The deviation in the initial part of the chain is due to the evanescent wave in experiments, which the numerical eigenanalysis does not incorporate.

Last, we derive analytical expressions for the frequencies of the TP modes by utilizing the symmetries of their eigenmodes, which are evident through their spatial waveform (bottom panel in Fig. 4). Let K_h and K_s denote the linear stiffness corresponding to hard (10°) and soft (20°) contacts. For the hard-hard interface, we observe from the mode shape that alternate particles do not move, while the rest of the particles oscillate around their equilibrium positions. Thus, considering that their net stiffness is $K_h + K_s$, the frequency of the TP mode in this hard-hard case would be $f_h = (1/2\pi)\sqrt{(K_h + K_s)/m}$. Similarly, for the soft-soft interface, one can derive that the frequency is $f_s = (1/2\pi)\sqrt{2K_s(1+\gamma^{-1})/m}$, where $\gamma = (3r - 1 + \sqrt{9r^2 - 14r + 9})/[2(r-1)]$ with $r = K_h/K_s$ (see Supplemental Material for further details [32]). We compare these analytical frequencies with the experimental values extracted directly from the spectrum plots in Fig. 4 and the numerical ones obtained from the eigenanalysis. For the current configuration, we find the frequency of the hard-hard TP mode is 12.18 (theory), 12.18 (numerics), and 12.15 ± 0.19 kHz (experiment). Similarly, the frequency of the soft-soft TP mode is 11.80 (theory), 11.80 (numerics), and 11.70 ± 0.08 kHz (experiment). Here, the standard deviations in experiments are based on the frequencies measured from all cylinder locations.

Judging from the agreement of analytical frequencies with computational and experimental results, these mathematical expressions can be used for distinguishing the TP modes from trivial defect modes. We see that for any values of K_h and K_s (complying with $K_h > K_s$), the interface modes exist and the corresponding frequencies reside *inside* the band gap without coalescing with the bulk bands. Hence, the modes are protected as long as we have a topological defect (hard-hard or soft-soft) created at the intersection of two topologically distinct dimer configurations. Again, these TP modes are robust against perturbations near the interface in contrast to trivial defect modes, and we verify the nature of the TP modes via numerics in Supplemental Material [32] (see also other related works, such as Refs. [39–41], on 1D topological interface modes).

Conclusions.—In this work, we proposed a highly tunable mechanical system made of cylindrical granular

particles, which can demonstrate an *in situ* topological band transition in a controllable manner. Using noncontact laser vibrometry, we precisely captured the smooth topological transition and showed how it leads to the emergence of a boundary mode in the system. We demonstrated the existence of topologically protected modes at the interface of two topologically distinct dimer configurations. The experimental observations of the resulting modes are supported by the theory and numerics. We also confirmed that these topologically protected modes are robust under perturbations, unlike trivial defect modes observed in granular chains. Though the current study is limited to linear dynamics, the proposed system can be tuned to incorporate nonlinear effects. In that light, this framework can provide a promising test bed for future studies involving the interplay of nonlinearity and topologically protected modes.

We gratefully acknowledge discussions with Professor Michael Weinstein, Columbia University, and Dr. Krishanu Roychowdhury, Cornell University. J. Y. is grateful for the support from NSF (CAREER-1553202) and ONR (N000141410388). J. Y. and P. G. K. thank the support of ARO (W911NF-15-1-0604). P. G. K. also acknowledges support from NSF-PHY-1602994, the Alexander von Humboldt Foundation, and the Stavros Niarchos Foundation via the Greek Diaspora Fellowship Program. E. K. thanks the support from the National Research Foundation of Korea (NRF) grant funded by the Korea government (MSIP, No. 2017R1C1B5018136).

R. C. and E. K. contributed equally to this work.

*Corresponding author.
jkyang@aa.washington.edu

[1] M. Z. Hasan and C. L. Kane, Rev. Mod. Phys. **82**, 3045 (2010).
[2] X. L. Qi and S. C. Zhang, Rev. Mod. Phys. **83**, 1057 (2011).
[3] R. Süsstrunk and S. D. Huber, Science **349**, 47 (2015).
[4] L. M. Nash, D. Kleckner, A. Read, V. Vitelli, A. M. Turner, and W. T. M. Irvine, Proc. Natl. Acad. Sci. U.S.A. **112**, 14495 (2015).
[5] P. Wang, L. Lu, and K. Bertoldi, Phys. Rev. Lett. **115**, 104302 (2015).
[6] S. H. Mousavi, A. B. Khanikaev, and Z. Wang, Nat. Commun. **6**, 8682 (2015).
[7] R. K. Pal, M. Schaeffer, and M. Ruzzene, J. Appl. Phys. **119**, 084305 (2016).
[8] R. K. Pal and M. Ruzzene, New J. Phys. **19**, 025001 (2016).
[9] S. D. Huber, Nat. Phys. **12**, 621 (2016).
[10] F. D. M. Haldane and S. Raghu, Phys. Rev. Lett. **100**, 013904 (2008).
[11] M. C. Rechtsman, J. M. Zeuner, Y. Plotnik, Y. Lumer, D. Podolsky, F. Dreisow, S. Nolte, M. Segev, and A. Szameit, Nature (London) **496**, 196 (2013).
[12] Y. Plotnik, M. C. Rechtsman, D. Song, J. M. Zeuner, A. Szameit, M. Segev, and Z. Chen, Nat. Mater. **13**, 57 (2014).
[13] M. J. Ablowitz and Y.-P. Ma, Opt. Lett. **40**, 4635 (2015).
[14] J. P. Lee-Thorp, I. Vukicevic, X. Xu, J. Yang, C. L. Fefferman, C. W. Wong, and M. I. Weinstein, Phys. Rev. A **93**, 033822 (2016).
[15] W. P. Su, J. R. Schrieffer, and A. J. Heeger, Phys. Rev. Lett. **42**, 1698 (1979).
[16] J. Zak, Phys. Rev. Lett. **62**, 2747 (1989).
[17] M. Atala, M. Aidelsburger, J. T. Barreiro, D. Abanin, T. Kitagawa, E. Demler, and I. Bloch, Nat. Phys. **9**, 795 (2013).
[18] Y. Hadad, A. B. Khanikaev, and A. Alù, Phys. Rev. B **93**, 155112 (2016).
[19] C. L. Kane and T. C. Lubensky, Nat. Phys. **10**, 39 (2013).
[20] R. Süsstrunk and S. D. Huber, Proc. Natl. Acad. Sci. U.S.A. **113**, E4767 (2016).
[21] A. C. Hladky-Hennion, G. Allan, and M. De Billy, J. Appl. Phys. **98**, 054909 (2005).
[22] A. C. Hladky-Hennion and M. de Billy, J. Acoust. Soc. Am. **122**, 2594 (2007).
[23] J. F. Robillard, O. B. Matar, J. O. Vasseur, P. A. Deymier, M. Stippinger, A. C. Hladky-Hennion, Y. Pennec, and B. Djafari-Rouhani, Appl. Phys. Lett. **95**, 124104 (2009).
[24] F. Casadei, T. Delpero, A. Bergamini, P. Ermanni, and M. Ruzzene, J. Appl. Phys. **112**, 064902 (2012).
[25] N. Swinteck, P. Lucas, and P. A. Deymier, AIP Adv. **4**, 124603 (2014).
[26] K. L. Johnson, *Contact Mechanics* (Cambridge University Press, Cambridge, England, 1985).
[27] D. Khatri, D. Ngo, and C. Daraio, Granular Matter **14**, 63 (2012).
[28] F. Li, D. Ngo, J. Yang, and C. Daraio, Appl. Phys. Lett. **101**, 171903 (2012).
[29] R. Chaunsali, F. Li, and J. Yang, Sci. Rep. **6**, 30662 (2016).
[30] E. Kim, F. Li, C. Chong, G. Theocharis, J. Yang, and P. G. Kevrekidis, Phys. Rev. Lett. **114**, 118002 (2015).
[31] P. A. Cundall and O. D. L. Strack, Geotechnique **29**, 47 (1979). In this study, our system composed of cylindrical particles can adopt the discrete element model, because the local resonant frequencies of the particles are significantly higher than the operating frequency of the system.
[32] See Supplemental Material at http://link.aps.org/supplemental/10.1103/PhysRevLett.119.024301 for a detailed description of the eigenanalysis and the Zak phase calculation, differences between the presented granular system and the SSH system, experimental results on the topological band transition, and robustness of topologically protected modes, which includes Refs. [15–17,26,27,33,35].
[33] J. K. Asbóth, L. Oroszlány, and A. Pályi, arXiv:1509.02295.
[34] C. Kittel, *Introduction to Solid State Physics* (Wiley, New York, 2005).
[35] M. Xiao, G. Ma, Z. Yang, P. Sheng, Z. Q. Zhang, and C. T. Chan, Nat. Phys. **11**, 240 (2015).
[36] P. B. Allen, S. Aubin, and R. B. Doak, Am. J. Phys. **68**, 228 (2000).
[37] R. F. Wallis, Phys. Rev. **105**, 540 (1957).

[38] A. Blanco-Redondo, I. Andonegui, M. J. Collins, G. Harari, Y. Lumer, M. C. Rechtsman, B. J. Eggleton, and M. Segev, Phys. Rev. Lett. **116**, 163901 (2016).

[39] C. L. Fefferman, J. P. Lee-Thorp, and M. I. Weinstein, Proc. Natl. Acad. Sci. U.S.A. **111**, 8759 (2014).

[40] Y. X. Xiao, G. Ma, Z. Q. Zhang, and C. T. Chan, Phys. Rev. Lett. **118**, 166803 (2017).

[41] E. Prodan, K. Dobiszewski, A. Kanwal, J. Palmieri, and C. Prodan, Nat. Commun. **8**, 14587 (2017).